ACS APPLIED MATERIALS & INTERFACES

Letter

www.acsami.org

Tunable Surface Plasmon Resonance and Strong SERS Performances of Au Opening-Nanoshell Ordered Arrays

Guangqiang Liu,* Yue Li, Guotao Duan, Jingjing Wang, Changhao, Liang, and Weiping Cai*

Key Lab of Materials Physics, Anhui Key Lab of Nanomaterials and Nanotechnology, Institute of Solid State Physics, Chinese Academy of Sciences, Hefei 230031, P.R. China

ABSTRACT: Au opening-nanoshell ordered arrays with tunable local surface plasmon resonance (SPR) property have been fabricated based on sputtering deposition onto monolayer colloidal crystal. The changes in local SPR peak for the arrays can be well tuned from visible to near-infrared region with decreasing of the spacing between two neighbor opening-nanoshells. It has been revealed that the changes of SPR peak originate from the electromagnetic coupling between two adjacent Au opening-nanoshells. This study is important to design and fabricate surface-enhanced Raman scattering substrates with high activity and practical application.

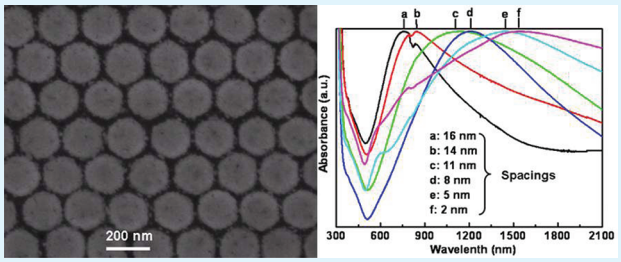

KEYWORDS: *Au opening-nanoshell, ordered arrays, sputtering deposition, tunable SPR, electromagnetic Coupling, SERS*

1. INTRODUCTION

Surface enhanced Raman Scattering (SERS) effect depends on a potentially large enhancement in the effective Raman cross-section of trace molecules located at or very close to a certain roughened noble metal surface or colloidal metal particles, and is recognized as one of the most promising applications.[1−3] Two phenomena contribute to the SERS effect: one is the electromagnetic effect that relies on local surface plasmon resonance (SPR) and makes a major contribution to SERS;[4] and the other is the chemical effect originating from formation of the charge-transfer complexes.[5] The electromagnetic coupling between two nanosized objects plays an important role in SERS effect, which increases significantly with reduction of the spacing between them.[6] The nanogap between two nano-objects is usually called "hot spots".[7] However, fine-control of the nanogap's size is still quite difficult because of the lack of effective method.

Nanoshells of noble metal, especially for Au, have attracted much attention because of their controllable local SPR properties by adjusting their structural parameters (curvature and thickness). And also, Au nanoshell possesses a good biological compatibility and has a potential application in thermotherapy.[8−12] Compared with an Au hollow sphere with nanosized shell, Au opening-nanoshell can exhibit enhanced optical absorption and scattering cross sections at higher wavelength.[13−16] If using the array, consisting of Au opening-nanoshell, as a SERS substrate, it should has an advantage of high structural uniformity, which is highly valuable to design devices detecting organic molecules with stable performance, in addition to the strong electromagnetic coupling between nanoshelled-objects in the array.

The template technology based on a monolayer colloidal crystal gives us a flexible tool to fabricate periodically structured arrays, which can ensure the structural uniformity on a whole substrate.[17−26] However, tuning the local SPR of noble metals in a large range, especially to the near-infrared (NIR) region, is still a challenge. Local SPR in NIR region for an array is very important for fiber-optic SERS sensors.[27,28] The reason is mainly as follows: (i) transmission of the SERS signal has little loss at the NIR region because of the absorption window; (ii) excitation at a wavelength in the NIR region can reduce the effects of native autofluorescence and absorption on the SERS signal output; (iii) the array can also be used for biomedical application based on SERS effect because the blood and tissue are most transparent in this region.

In this paper, we fabricate the Au opening-shell arrays based on sputtering deposition of Au onto monolayer polystyrene (PS) colloidal crystal, or the strategy shown in Figure 1. Briefly, a hexagonally close-packed PS colloidal monolayer on a silicon substrate (Figure 1A) is first bombarded or etched by argon plasma to obtain nonclose-packed colloidal monolayer (Figure 1B).[29−31] A thin gold layer is then coated on the etched PS sphere surfaces via a plasma sputtering deposition (Figure 1C). Because of the area contact of the PS spheres with the substrate, which can be controlled by heating, Au opening-nanoshell ordered arrays can be thus obtained after removal of PS colloidal template (Figure 1D). The structural parameters of the array (shell-thickness, curvature, opening size and spacings between adjacent nanounits) can be controlled by deposition and template conditions. So the SPR and SERS performances can be tunable.

Received: March 30, 2011
Accepted: December 15, 2011
Published: December 15, 2011

   dx.doi.org/10.1021/am201455x | *ACS Appl. Mater. Interfaces* 2012, 4, 1−5

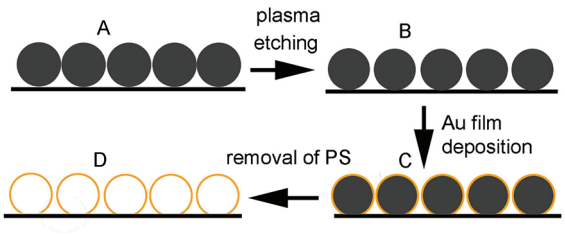

Figure 1. Schematic illustration of formation of Au opening-nanoshell arrays: (A) close-packed PS colloidal monolayer on silicon substrate; (B) Non-close-packed PS colloidal monolayer after argon plasma etching of the close-packed one; (C) a thin gold layer coated on the etched colloidal monolayer by ion-sputtering deposition; (D) Au opening-nanoshell array after removal of PS spheres.

2. EXPERIMENTAL SECTION

2.1. Sample Preparation. According to the strategy shown in Figure 1, the uniform PS monolayer colloidal crystals with close-packing were first prepared on a well cleaned glass substrate with 2 × 2 cm in size by spin coating of the PS colloidal suspension. The formed PS monolayer colloidal crystals were then transferred onto a cleaned silicon substrate using water as medium, as previously described.[33] The close-packed colloidal monolayer was etched by argon plasma for 6 min (PDC-32G-2, at a pressure of 0.2 mbar and an input power of 100 mW) to obtain nonclose-packed template.[34] A thin gold layer was deposited on the etched PS colloidal monolayer via plasma sputtering at a rate of 6 nm min^{-1} in thickness. The thickness of gold layer was controlled by the sputtering deposition time. The colloidal monolayer with the gold coating were immersed in methylene chloride (CH_2Cl_2) solution for 10 min to dissolve the PS spheres, as previously reported,[35] and an Au nanoshell array was finally left after being cleaned with distilled water several times and dried with high-purity flowing nitrogen.

2.2. Sample Characterization. The morphology of samples was observed on a field-emission scanning electronic microscope (FESEM, sirion 200 FEG). For transmission electron microscopic (TEM, JEOL 2010, at 200KV) examination, the products were scrapped from the substrate, dispersed in ethanol by supersonic vibration and finally transferred on the carbon-coated copper grid. Optical absorption spectra were recorded on a spectrophotometer (Cary 5E UV/vis−NIR) in the wavelength range from 200 to 1000 nm.

For Raman spectral measurements, the samples were immersed in 1 × 10^{-6} M 4-aminothiophenol (4-ATP) solution for 10 min, and then picked up and dried with high-purity flowing nitrogen. The Raman spectra were recorded with a portable Raman spectrometer (MiniRam III), using a laser beam with an excitation wavelength of 785 nm (integrate time 10 s).

3. RESULT AND DISCUSSION

3.1. Arrays' Structure and Tunable SPR. After the gold layer-coated samples were immersed in CH_2Cl_2 solution for 10 min, the PS spheres would be dissolved completely and left the hollow structure, as illustrated in Figure 3A in ref 35). Figure 2A shows a typical FESEM image of the as-prepared sample, from the PS spheres with initial size 200 nm, after sputtering deposition for 24 s (2.4 nm in deposition thickness) and removal of PS spheres. It exhibits a hexagonal nonclose packed array. The gaps or spacings between two adjacent units in the

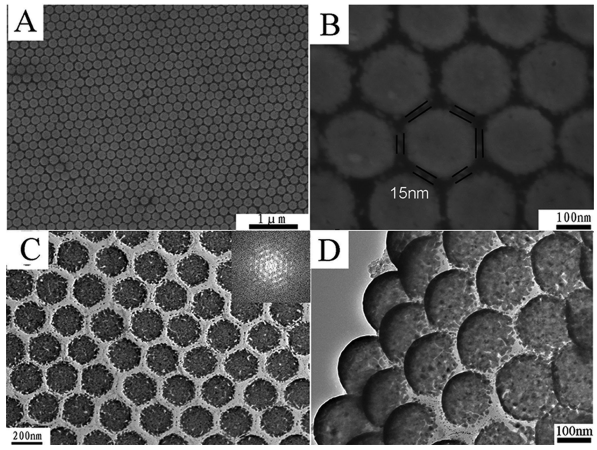

Figure 2. Morphology of the Au opening-nanoshell array obtained from the colloidal monolayer template with 200 nm in PS diameter and deposition for 24 s. (A) Typical FESEM image; (B) local magnified image of A; (C) TEM image of the sample shown in A, and the inset is the corresponding fast Fourier transform (FFT); (D) TEM image observed with a slantwise angle for the sample shown in A.

array are about 15 nm, and there were six symmetrical gaps around each unit, as shown in Figure 2B. The number density of the gaps is about 1 × 10^{10}/cm^2. The density can be controlled by the initial size of PS spheres in the template. Figure 2C is the corresponding TEM image of the sample after scraping from the substrate. It still keeps hexagonal nonclose packed arrangement. The inset is the corresponding fast Fourier transform (FFT), and the diffraction pattern should origin from the periodical structure of the Au array, which indicates the hexagonal-packed structure. Meanwhile, we obtained the TEM image of slightly slantwise arrays (as shows in Figure 2D), from which we can identify the shell structure of each unit, according to the thick brim and the thin midst. And each unit in the array is an incomplete hollow sphere with a "placket" at bottom. So, we called it opening-shell structure. This is attributed to nonshadow-depostion on PS spheres under plasma sputtering.[35] Further, the gaps or the spacings between neighboring two opening-nanoshells can be tuned by the sputtering-deposition time. Figure 3 shows the spacings from ∼5 nm to ∼20 nm, corresponding to the different sputtering-deposition time.

Correspondingly, we can examine the spacing-dependent SPR. Figure 4A shows the optical absorbance spectra for the Au opening-shell arrays with the spacings ranged from 16 nm to 2 nm (corresponding to the shell thicknesses from 2 to 9 nm, estimated according to the deposition rate of 6 nm/min). There exists a local SPR peak around 760 nm for the sample with 16 nm in the spacing (or 2 nm in shell thickness). The SPR can red-shift to 1530 nm (in NIR region) with decreasing of the spacing from 16 nm to 2 nm or increasing of the shell thickness from 2 nm to 9 nm. The SPR position shows near linear dependence on the spacings between two adjacent units in such arrays, as illustrated in Figure 4B (the data from Figure 4A).

Such spacing or shell thickness dependent SPR is different from the previous reports,[9,11] for the isolated Au shells (or hollow particles), which showed the SPR shifting to short wavelength with increasing the shell thickness. Therefore, the SPR in this study should not mainly originate from a single Au opening-nanoshell. In fact, increasing of shell thickness

dx.doi.org/10.1021/am201455x | ACS Appl. Mater. Interfaces 2012, 4, 1−5

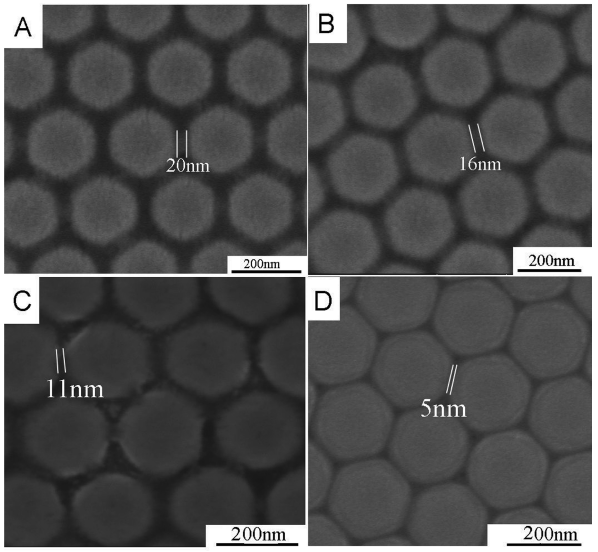

Figure 3. FESEM images of the Au opening-nanoshell arrays obtained by sputtering deposition for different time.(A) 5, (B) 20, (C) 45, and (D) 75 s.

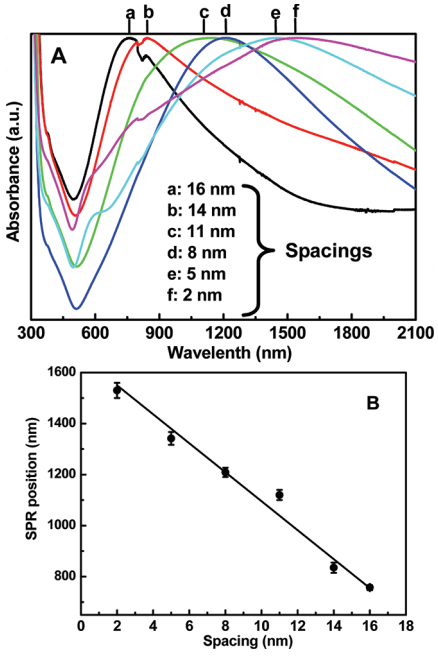

Figure 4. Optical absorption properties for the Au opening-nanoshell arrays with different spacings or shell-thickness. (A) Absorbance spectra; (B) SPR position as a function of the spacing (for the data in A, the line is a guide to aid the eye).

corresponds to reduction of the spacing between the adjacent nanounits in the arrays. It is such reduced spacing that induces the electromagnetic plasmonic coupling of the adjacent Au opening-shells. Such the coupling effect can enhance electromagnetic fields at the nanogap sites.[36−38] Usually, the SPR peak will red-shift with decreasing the spacing between adjacent nanounits according to the equation[25,39]

$$\frac{\Delta\lambda}{\lambda_0} = a\exp\left(-\frac{d}{bD}\right) \quad (1)$$

Where λ_0 is the SPR wavelength in the uncoupling case, $\Delta\lambda$ the red-shift of SPR in wavelength; a and b are the fitting parameters (>0); D and d the size of a nanounit and the spacing between two adjacent ones, respectively. Obviously, $\Delta\lambda$ increases with decreasing the value of d (see Figure 4A). Further, when $d/(bD) \ll 1$, eq 1 can be written as

$$\Delta\lambda \approx A - Bd \quad (2)$$

where A and B are the contants associated with a, b, D, and λ_0. In this case, the SPR shift $\Delta\lambda$ exhbits near linear dependence on the spacings. It means that eq 2 can well-describe the results shown in Figure.4B.

3.2. Dependence of SERS Effect on SPR. It is well-known that when the excitation is carried out at a wavelength near the SPR position, the achieved SERS signal will be the strongest.[32,40] However, the accurate tuning of the SPR around the position of the excitation wavelength is still a challenge because of lack of effective method to control the local SPR wavelength. The method presented in this study can easily realize it. Here we take the normal Raman excitation wavelength of 785 nm as example to demonstrate the feasibility of accurate-tuning the SPR position and to show the dependence of the SERS activity on the SPR wavelength. We can easily control the SPR at 785 nm for the Au-opening nanoshell array just by sputtering deposition time (24 s), as indicated in curve c of Figure 5A, corresponding to the sample

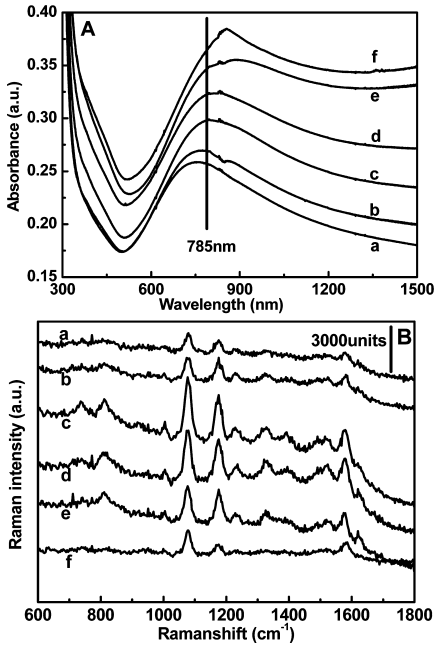

Figure 5. Comparison between (A) optical absorption spectra, for Au opening-nanoshell arrays with different fine-tuned shell thicknesses, and (B) Raman spectra of 4-ATP on the arrays. Curves a−f: the arrays by sputtering deposition for 22, 23, 24s, 25, 26, and 27 s, respectively. Excitation wavelength for Raman spectra: 785 nm.

shown in Figure.2. For comparison, we also fabricated the other Au opening-nanoshell arrays with the SPR near the excitation wavelength (785 nm) by sputtering deposition for different time, as illustrated in curves a, b, and d−f of Figure 5A. Figure 5B shows the Raman spectra of 4-ATP molecules absorbed on these arrays with the SPR positions shown in Figure 5A, correspondingly. Although there is still some controversy about the relation among the excitation wavelength, SPR and SERS signal,[40,41] in our experiment, we can see that the SERS signal is the most intense when the SPR is located at site of the

dx.doi.org/10.1021/am201455x | ACS Appl. Mater. Interfaces 2012, 4, 1−5

excitation wavelength, as shown in curve c of Figure 5B. This should be easily understood. When exciting at the position of SPR peak, the strongest electromagnetic plasmonic coupling will take place and induce the strongest SERS signal. Further experiments have revealed that the measurement reproducibility of the SERS signal is very good across the samples, as shown in Figure 6. This is attributed to the highly homogeneous structure of such ordered arrays.

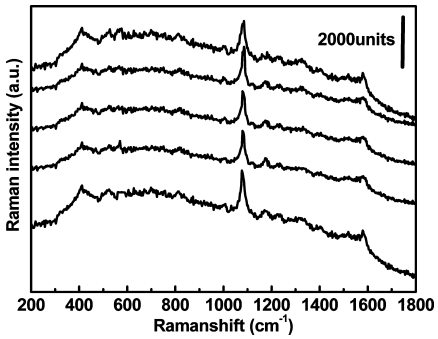

Figure 6. Raman spectra of 4-ATP at five different spots on the sample obtained by sputtering deposition for 27 s.

This array, used for SERS substrate, has the following advantages: (i) It has an even surface, which can ensure the uniformity of SERS signal across whole substrate, and stability for the device application based on SERS effect. (ii) There exist many gaps, in this array, as "hot spots" for SERS substrate. Recently, there are some reports on noble metals (Ag and Au) within anodic aluminum oxide template as SERS substrate because of its high number density of pores (about 1×10^{10}/cm^2).[42] Compared with that substrate, our Au-nanoshell arrays have high number density of nanogaps similarly, and hence are of high SERS activity. (iii) The local SPR property of this array can be tuned from visible to near-infrared region easily by changing the spacing between two adjacent nanounits. Therefore we can control fabrication of the appropriate sample with the SPR position in accord with the exciation wavelength.

4. CONCLUSIONS

In summary, we have developed a method to prepare Au opening-nanoshell arrays by sputtering deposition based on colloidal monolayer template. The gaps between adjacent nanoshells can be well controlled, further resulting in fine-tunability of local SPR property of such arrays. The local SPR originates mainly from the electromagnetic coupling between two adjacent Au opening-nanoshells and can be tuned from visible to NIR region by changing the spacings between two adjacent Au nanoshells. This array can be used as the substrate with high SERS activity and very homogeneous SERS activity. If using the smaller PS colloidal crystals, we can obtain nanogaps with the higher number density. Similarly, we can also fabricate Ag opening-nanaoshell ordered arrays. This work is of significance in designing and fabrication of SERS substrates with high performances, and especially, in practical application of the fiber-optic SERS sensors.

AUTHOR INFORMATION

Corresponding Author

*E-mail: liugq@issp.ac.cn (G.L.); wpcai@issp.ac.cn (W.C.).

ACKNOWLEDGMENTS

The authors acknowledge the National Basic Research Program of China (973 Program, Grant No. 2011CB302103), the financial supports from Natural Science Foundation of China (Grant No. 10704075, 10974203 and 50831005), and provincial Natural Science Foundation of Anhui (Grant No. 11040606M62).

REFERENCES

(1) Tao, A.; Kim, F.; Hess, C.; Goldberger, J.; He, R. G.; Sun, Y. G.; Xia, Y. N.; Yang, P. D. *Nona Lett.* **2003**, *3*, 1229−1233.
(2) Xiong, Y.; Mclellan, J. M.; Chen, J.; Yin, Y.; Li, Z. Y.; Xia, Y. N. *J. Am. Chem. Soc.* **2005**, *127*, 17118−17127.
(3) Stuart, D. A.; Kevin, B. B.; Van Duyne, R. P. *Analyst* **2006**, *131*, 568−572.
(4) Moskovits, M. *J. Raman Spectrosc.* **2005**, *36*, 485−496.
(5) Campion, A.; Kambhampati, P. *Chem. Soc. Rev.* **1998**, *27*, 241−250.
(6) Jiang, J.; Bosnick, M.; Brus, L. *J. Phys. Chem. B.* **2003**, *107*, 9964−9972.
(7) Nie, S. M.; Emory, S. R. *Science* **1997**, *275*, 1102−1106.
(8) Liu, G. L.; Liu, Y.; Kim, J.; Doll, J. C.; Lee, L. P. *Adv. Mater.* **2005**, *17*, 2683−2688.
(9) Zimmermann, C.; Feldmann, C.; Wanner, M.; Gerthsen, D. *Small* **2007**, *3*, 1347−1349.
(10) Prevo, B. G.; Esakoff, S. A.; Mikhailovsky, A.; Zasadzinski, J. A. *Small* **2008**, *4*, 1183−1195.
(11) Zeng, J.; Huang, J. L.; Lu, W.; Wang, X. P.; Wang, B.; Zhang, S. Y.; Hou, J. G. *Adv. Mater.* **2007**, *19*, 2172−2176.
(12) Liang, H. P.; Wan, L. J.; Bai, C. L.; Jiang, L. *J. Phys. Chem. B.* **2005**, *109*, 7795−7800.
(13) Love, J. C.; Gates, B. D.; Wolfe, D. B.; Paul., Kateri. E.; Whitesides, G. M. *Nano Lett.* **2002**, *2*, 891−894.
(14) Charnay, C.; Lee, A.; Man, S. Q.; Moran, C. E.; Radloff, C.; Bradley, R. K.; Halas, N. J. *J. Phys. Chem. B.* **2003**, *107*, 7327−7333.
(15) Ye, J.; Van Dorpe, P.; Van Roy, W.; Lodewijks, K.; De Vlaminck, I.; Maes, G.; Borghs, G. *J. Phys. Chem. C.* **2009**, *113*, 3110−3115.
(16) Ye, J.; Van Dorpe, D. P.; Van Roy, W.; Maes, G.; Borghs, G. *Langmuir* **2009**, *25*, 1822−1827.
(17) Liu, X. F.; Linn, N. C.; Sun, C.-H.; Jiang, P. *Phys. Chem. Chem. Phys.* **2010**, *12*, 1379−1387.
(18) Wang, C. X.; Ruan, W. D.; Ji, N.; Ji, W.; Lv, S.; Zhao, C.; Zhao, B. *J. Phys. Chem. C.* **2010**, *114*, 2886−2890.
(19) Baia, L.; Baia, M.; Popp, J.; Astilean, S. *J. Phys. Chem. B* **2006**, *110*, 23982−23986.
(20) Farcâu, C.; Astilean, S. *Appl. Phys. Lett.* **2009**, *95*, 193110−193113.
(21) Liu, J. Q.; McBean, K. E.; Harris, N.; Cortie, M. B. *Mater. Sci. and Engi. B* **2007**, *140*, 195−198.
(22) Li, Y.; Naoto, K.; Cai, W. P. *Coord. Chem. Rev.* **2010**, *255*, 357−373.
(23) Li, Y.; Cai, W. P.; Duan, G. T. *Chem. Mater.* **2008**, *20*, 615−624.
(24) Li, L.; Zhai, T. Y.; Zeng, H. B.; Fang, X. S.; Bando, Y; Dmitri Golberg., J. *Mater. Chem.* **2011**, *21*, 40−56.
(25) Zhang, J. H.; Yang, B. *Adv. Funct. Mater.* **2010**, *20*, 3411−3424.
(26) Masson, J.-F.; Gibson, K. F.; Provencher-Girard, A. *J. Phys. Chem. C* **2010**, *114*, 22406−22412.
(27) Konorov, S. O.; Addison, C. J.; Schulze, H. G.; Turner, R. F. B.; Blades, M. W. *Opt. Lett.* **2006**, *31*, 1911−1913.
(28) Geßner, R.; Rösch, P; Petry, R; Schmitt, M.; Strehle, M. A.; Kiefer, W.; Popp, J. *Analyst.* **2004**, *129*, 1193−1199.
(29) Yi, L.; Lauardi, L. M.; Muth, J. P. *IEEE Sens. J.* **2010**, *10*, 617−620.
(30) Murray-Methot, M. P.; Ratel, M.; Masson, J. F. *J. Phys. Chem. C* **2010**, *114*, 8268−8275.
(31) Murray-Methot, M. P.; Menegazzo, N.; Masson, J. F. *Analyst* **2008**, *133*, 1714−1721.

(32) Lee, S. H.; Bantz, K. C.; Lindquist, N. C.; Oh, S. H.; Haynes, C. L. *Langmuir* **2009**, *25*, 13685−13693.
(33) Sun, F; Cai, Q.; Li, W. P.; Cao, Y.; Lei, B. Q.; Zhang, Y. *L. D. Adv. Funt. Mater.* **2004**, *14*, 283−288.
(34) Yang, J. L.; Duan, G. T.; Cai, W. P. *J. Phys. Chem. C* **2009**, *113*, 3973−3977.
(35) Duan, G. T.; Lv, F. J.; Cai, W. P.; Luo, Y. Y.; Li, Y.; Liu, G. Q. *Langmuir* **2010**, *26*, 6295−6302.
(36) Olk, P.; Renger, J.; Härtling, T.; Wenzel, M. T.; Eng, L. M. *Nano Lett.* **2007**, *7*, 1736−1740.
(37) Talley, C. E.; Jackson, J. B.; Oubre, C.; Grady, N. K.; Hollars, C. W.; Lane, S. M.; Huser, T. T.; Nordlander, P.; Halas, N. J. *Nano Lett.* **2005**, *5*, 1569−1574.
(38) Härtling, I.; Alaverdyan, Y.; Hille, A.; Wenzel, M. T.; Käll, M.; Eng, L. M. *Opt. Express* **2008**, *16*, 12362−12371.
(39) Jain, P. K.; El-Sayed, M. A. *Chem. Phys. Lett.* **2010**, *487*, 153−164.
(40) McFarland, A. D.; Young, M. A.; Dieringer, J. A.; Van Duyne, R. P. *J. Phys. Chem. B* **2005**, *109*, 11279−11285.
(41) Gibson, K. F.; Correia-Ledo, D.; Couture, M.; Graham, D.; Masson, J. F. *Chem. Commun.* **2011**, *47*, 3404−3406.
(42) Ko, H.; Chang, S.; Tsukruk, V. *ACS. Nano* **2009**, *3*, 181−188.